ACS APPLIED MATERIALS & INTERFACES

Research Article

Cite This: ACS Appl. Mater. Interfaces 2019, 11, 7030−7036

www.acsami.org

Different Protonic Species Affecting Proton Conductivity in Hollow Spherelike Polyoxometalates

Wen-Jing Liu,[†] Long-Zhang Dong,[†] Run-Han Li,[†] Yong-Jun Chen, Sheng-Nan Sun, Shun-Li Li, and Ya-Qian Lan*

Jiangsu Key Laboratory of Biofunctional Materials, School of Chemistry and Materials Science, Nanjing Normal University, Nanjing 210023, P. R. China

Supporting Information

ABSTRACT: Polyoxometalates (POMs), which possess strong acidity and chemical stability, are promising solid proton conductors and potential candidates for proton exchange membrane fuel cell applications. To investigate how factors such as proton concentration and carrier affect the overall proton conduction, we have synthesized new compounds $HImMo_{132}$ (Im, imidazole), $HMeImMo_{132}$, $ILMo_{132}$, and $TBAMo_{132}$ with hollow structures and $HImPMo_{12}$ with a solid spherelike structure. These crystal models were prepared by encapsulating POM with organic molecules with different proton contents. Among them, the single-crystal sample of the hollow structure $HImMo_{132}$ containing more proton sources shows a high proton conductivity of 4.98×10^{-2} S cm^{-1}, which was approximately 1 order of magnitude greater than that of the solid cluster $HImPMo_{12}$ with the same proton sources and 3 orders of magnitude greater than that of the proton-free organic cation-encapsulated giant ball $TBAMo_{132}$. This study provides a theoretical guidance toward designing and developing new-generation proton conductors and studying their performances at the molecular level.

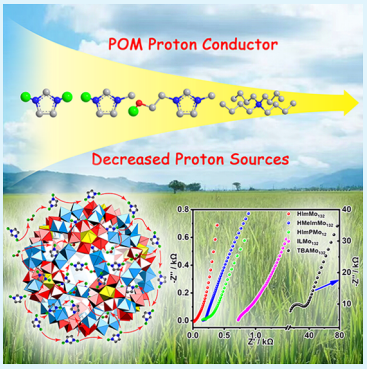

KEYWORDS: *polyoxometalate, proton conductor, hollow structure, single crystals, inorganic−organic hybrid*

1. INTRODUCTION

Conventional nonrenewable resources including coal, oil, and natural gas would generate a large amount of harmful substances during the combustion process and cause serious environmental contamination, greenhouse effect, etc. Fuel cells are electrochemical energy conversion devices that produce electricity from chemical energy of fuels such as hydrogen, oxygen, methanol, natural gas, etc.[1−8] Proton exchange membrane fuel cells (PEMFCs) are one of the most promising candidates among fuel cells for power applications in portable electronic devices and power stations due to their relatively low operating temperature and fast start-up and shut-down cycles.[9] As a crucial component of PEMFCs, a proton exchange membrane (PEM) should be designed to have high proton conductivity (>10^{-2} S cm^{-1}) to facilitate proton diffusion and good chemical stability to keep its structural integrity under variable operating conditions.[10,11] The use of the popular material Nafion was limited because of its high cost and low operation temperature (lower than 80 °C).[12,13] Most of the reported polymer proton materials and carbon-based proton conductor materials exhibit excellent proton conductivity, but it is difficult to study their conductive pathways and mechanisms at the molecular level.[14,15] This inspired us to find and design a model with crystal structures to simulate and understand the relationship between the structure and proton hopping/conductive pathways. Especially, a model containing a metal cluster and a hollow spherelike structure provides us with great opportunities to compare its proton conductivity performance at the molecular level, further offers insight into structure−property relationships, and furnishes theoretical guidance for the synthesis of new proton-conducting materials. Metal−organic frameworks (MOFs) with crystalline structures,[16−25] a potential candidate, allow us to study their proton-conducting pathways and mechanisms at the molecular level. However, the physicochemical stability of some MOF compounds is often lower than that of conventional inorganic molecular sieves and porous carbon materials, resulting in poor chemical stability. For example, MOF with poor stability in aqueous solution is difficult to expand its application in aqueous media. Therefore, exploring chemically stable, inexpensive, environmentally friendly, and highly proton-conductive conductors is in great demand.

Polyoxometalates (POMs), consisting of a group of metal−oxygen clusters with O-rich surfaces, strong Lewis and Brønsted acidity, and strong redox activity, are especially attractive candidates for their applications in proton conductors.[26−32] Nakamura introduced the first POM-based material, the classical Keggin compound $\{H_3PM_{12}O_{40}\}$ (M = Mo, W) as a solid electrolyte material in a H_2−O_2 fuel cell.[33] However, the main obstacle in applying POMs directly in the fuel cell is their high solubility in water, leading to their unstable status in high humidity and a serious reduction in

Received: November 21, 2018
Accepted: January 23, 2019
Published: January 23, 2019

Downloaded via NANJING NORMAL UNIV on January 6, 2020 at 09:14:51 (UTC).
See https://pubs.acs.org/sharingguidelines for options on how to legitimately share published articles.

 © 2019 American Chemical Society

DOI: 10.1021/acsami.8b20509
ACS Appl. Mater. Interfaces 2019, 11, 7030−7036

Scheme 1. (a) Structural Formulas of Organic Cations HIm, HMeIm, IL, and TBA and Sites That May Act as Proton Carriers; (b) Schematic Illustration of the Multishelled $HImMo_{132}$ Structure with the Inherent Porosity and the Counter-Imidazole Layer Inside and Outside the Ball, Where Each Imidazole has Two Protons (Green Ball); (c) Schematic Diagram of $HImMo_{132}$; the Giant Orange Ball Represents Mo_{132}

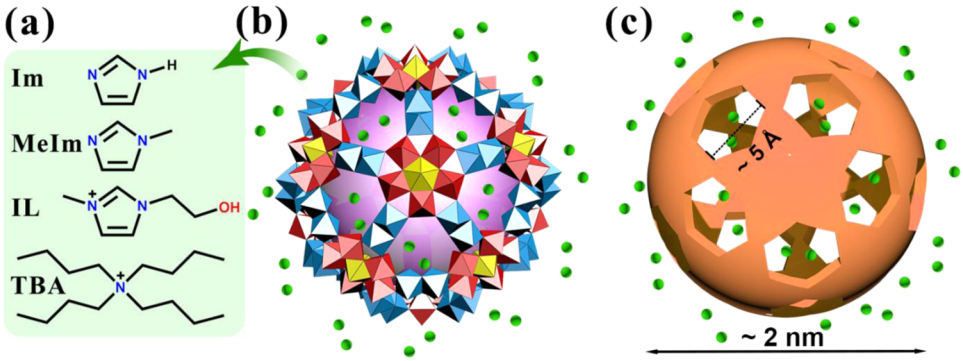

their specific surface area.[34] Besides, POM structures usually consist of numerous crystal waters, which are unstable and easy to lose, resulting in a rapid decrease in conductivity.[35] Therefore, researchers have been focusing their interest on synthesizing composites by combining both the advantages of POMs and other materials, thereby improving the overall proton conductivity performance.[36] For example, POMOF is formed by loading POM into the ordered channels of MOF to increase the jumping sites of the pores and improve the stability and hydrophilicity of the material.[37] By synthesizing POM-functionalized mesoporous silica through impregnation, Jiang found an association between the enhanced conductivity and the increased amount of POM.[38] However, these composites were synthesized by a very complex method with costly ingredients. To reduce the cost of synthetic materials and at the same time to solve the problem of instability of POMs under high humidity, we have designed a series of POM-based inorganic−organic hybrid materials rich in a proton source by a combination of the functional guest molecules containing the proton source (e.g., imidazole or ammonium cations) and POMs. Systematic explorations and comparisons of how different numbers of protons affect proton conductivity at the molecular level are crucial for better designing of new proton-conducting materials.

Herein, we report a family of organic cations encapsulating solid spherelike or giant hollow POMs in a very facile synthetic procedure with inexpensive starting materials, which could be obtained in large scale. Giant POM $\{Mo_{132}\}$ was chosen as the proton conductor here for the first time on the basis of the following considerations: first, $\{Mo_{132}\}$ possesses inherent existence of multiple transition metal centers in one molecule, excellent redox ability, ample surface oxygen sites, and outstanding electron-accepting capability. Second, the strong acidity nature and plenty terminal oxygen sites are helpful for the connection of hydrogen bond networks. Third, the giant POM has a hollow sphere with a diameter of 2 nm. There are 20 irregular hexagonal windows with a diameter of 5 Å in the structure, which is larger than that of the guest molecules, providing a channel for the proton-conducting pathway. More specifically, the utilization of organic cations such as imidazole and methylimidazole, which are capable of acting as cations and proton carriers or located inside the POM pore or between POM molecules, can further facilitate the proton transfer. As a result, investigation on the proton conductivity of the fullerenelike $\{Mo_{132}\}$ with different numbers of proton sources and compounds with the same protons in solid and hollow structures is discussed (Scheme 1). Among them, the imidazole-based POM with the formula $(HIm)_{24}(NH_4)_{20}[Mo_{72}{}^{VI}Mo_{60}{}^{V}O_{372}(CH_3COO)_{30}(H_2O)_{72}]\cdot ca190H_2O$ ($HIm_{24}Mo_{132}$) (Im, imidazole) shows high conductivity with the σ value of 4.98×10^{-2} S cm^{-1}.

2. EXPERIMENTAL SECTION

2.1. Synthesis of $(HIm)_{24}(NH_4)_{20}[Mo_{72}{}^{VI}Mo_{60}{}^{V}O_{372}(CH_3COO)_{30}(H_2O)_{72}]\cdot ca190H_2O$ ($HImMo_{132}$). All starting materials were commercially obtained and used in this work without further purification. $\{Mo_{132}\}$[1] was synthesized according to the previously reported literature. A sample of imidazolium (Im, 0.10 g, 1.50 mmol) was first dissolved in 10 mL of H_2O and then CH_3COOH was added dropwise until the pH value reached 4.0, followed by the addition of $\{Mo_{132}\}$ (0.59 g, 0.03 mmol). The resulting turbid dark brown suspension was transferred into a 15 mL Teflon-lined stainless steel autoclave and heated to 130 °C for 24 h and then cooled to room temperature at a rate of 3 °C h^{-1}. Dark brown, block crystals were collected and dried in air (yield 0.5 g, 61% based on $\{Mo_{132}\}$). IR (cm^{-1}): 1628(m), 1571(m), 1433(m), 1390(m) (δ_{CH_3}, $\nu_{s,COO}$, δ_{as}, NH_4^+), 1151(w), 967(s), 940(m) (ν(Mo═O)), 855(m), 798(s), 721(s), 626(m), 581(s). Elemental analysis (EA) % calcd (found): C 5.9 (6.0), H 2.9 (2.5), N 3.4 (4.0), inductively coupled plasma (ICP) analysis % calcd (found): Mo 46.8 (46.5). M = 27096 g mol^{-1}. The exact number of Ims and the number of guest crystal waters are calculated on the basis of elemental analysis, ICP analysis, and thermogravimetry analysis (TGA) data. For control experiment, material characterization, and crystallographic data in CIF, see the Supporting Information.

3. RESULTS AND DISCUSSION

The single crystals $HImMo_{132}$, $HMeIm_{132}$ (MeIm, 1-methylimidazolium), $ILMo_{132}$ (IL, 1-(2-hydroxyethyl)-3-methylimidazolium), $TBAMo_{132}$ (TBA, tetrabutylammonium), and $HImPMo_{12}$ were synthesized by metathesizing cations of the preprepared POMs to the respective organic molecules as countercations under the hydrothermal reaction at 130 °C and were characterized by single-crystal X-ray diffraction (XRD) structural analysis, elemental analysis (EA), inductively coupled plasma (ICP) analysis, Fourier transform infrared spectra (FT-IR), and thermogravimetry analysis (TGA) (see the Supporting Information, Tables S1, S2 and Figure S11). The introduction of organic cations into the anionic POM building units and finally into the specific crystal lattice arrangement gives us the opportunity to isolate the hydrophobic solid proton conductors. In the structure of polyanion

DOI: 10.1021/acsami.8b20509
ACS Appl. Mater. Interfaces 2019, 11, 7030−7036

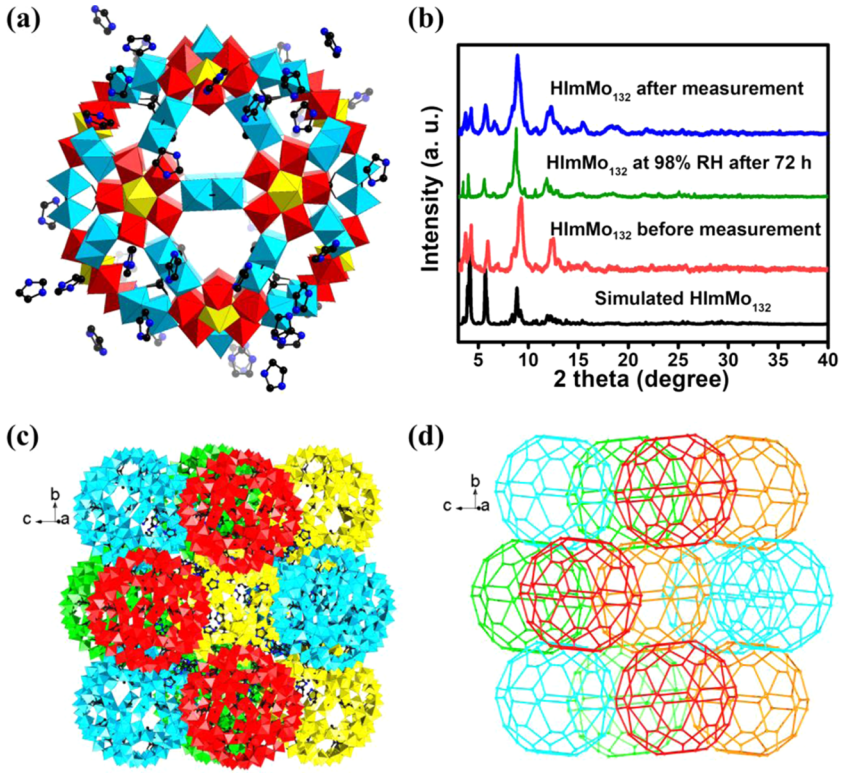

Figure 1. (a) Perspective view of the mesoporous cage of $HImMo_{132}$ with 5 Å hexagonal windows. (b) XRD pattern of $HImMo_{132}$. (c) View of the packing diagram of the $HImMo_{132}$ structure; imidazole groups are shown inside or outside the $\{Mo_{132}\}$ ball (color code: N, bule; C, black). (d) Truncated icosahedron with 12 regular pentagons formed by $\{(Mo^{VI})Mo_5^{VI}\}$ groups and 20 trigonal hexagons formed by the $\{(Mo_2^{V})_3(Mo^{VI})_3\}$ groups.

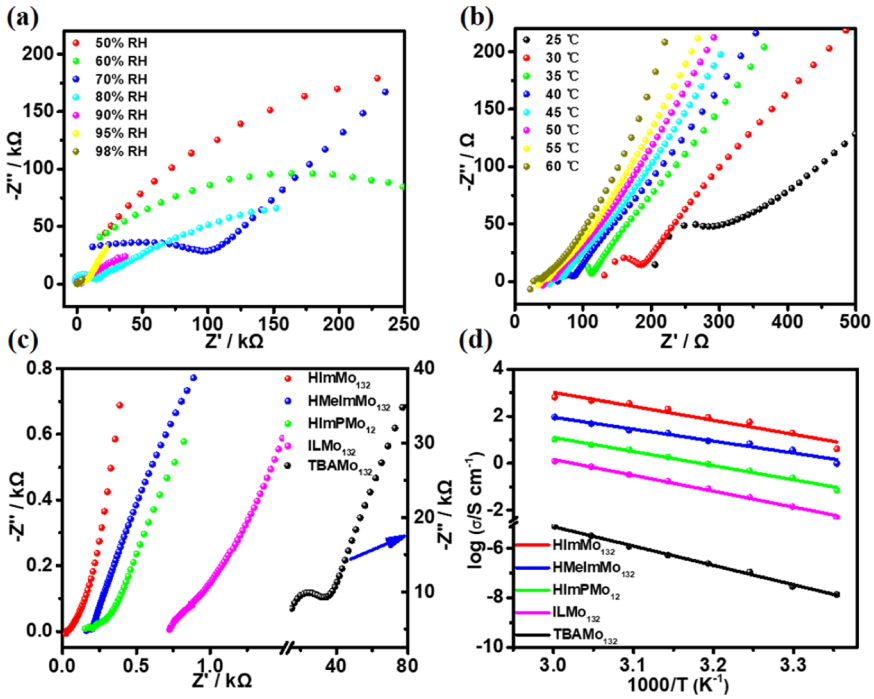

Figure 2. (a) Impedance spectra of $HImMo_{132}$ at 25 °C with different RHs. (b) Impedance spectra of $HImMo_{132}$ at 98% RH under various temperatures. (c) Comparison of impedance spectra for $HImMo_{132}$ (red), $HMeImMo_{132}$ (blue), $HImPMo_{12}$ (green), $ILMo_{132}$ (pink), and $TBAMo_{132}$ (black) under 60 °C with 98% RH. (d) Arrhenius plots of proton conductivity for $HImMo_{132}$, $HMeImMo_{132}$, $HImPMo_{12}$, $ILMo_{132}$, and $TBAMo_{132}$ under 98% RH conditions.

$[Mo_{132}]^{42-}$ (see Figure 1a), the pentagonal bipyramidal $\{(Mo^{VI}O_7)(Mo^{VI}O_6)_5\}$ subfragments are stabilized by 30 $\{Mo_2^{V}O_4(OOCCH_3)^+\}$ groups, resulting in a spherical object.[39] In the pentagonal units, the central $\{Mo^{VI}O_7\}$

DOI: 10.1021/acsami.8b20509
ACS Appl. Mater. Interfaces 2019, 11, 7030−7036

polyhedron is connected to five $\{Mo^{VI}O_6\}$ octahedra by edge share. The linker group $\{Mo_2^{V}\}$ is linked to two adjacent $\{Mo^{VI}O_6\}$ octahedra, and a total of three linker units $\{Mo_2^{V}\}$ and three octahedra $\{Mo^{VI}O_6\}$ from the pentagonal unit form one hexagon unit $\{(Mo_2^{V})_3(Mo^{VI})_3\}$ possessing an open window with a diameter of 5 Å. Compound $HImMo_{132}$ crystallizes in the orthorhombic space group *Pbca*. From the single-crystal XRD data, we can see that HIms are loaded into the cage of $\{Mo_{132}\}$ and distributed outside the pore of $\{Mo_{132}\}$ regularly. Based on EA, ICP, and TGA data, the loading number of organic cations such as HIm, HMeIm, IL, and TBA contained in each single cell of $HImMo_{132}$, $HMeIm_{132}$, $ILMo_{132}$, and $TBAMo_{132}$ is 24 (Figures S1−S4). Each $\{Mo_{132}\}$ group is surrounded by 24 protonated imidazole molecules and around 190 H_2O molecules through H-bonding. Figure 1c,d shows the packing diagram of $HImMo_{132}$ with an orderly arrangement forming a tunnel with zigzag profiles. Polyanion $[PMo_{12}]^{3-}$ is assembled by a central $\{PO_4\}$ tetrahedron surrounded by four corner-shared $\{Mo_3O_{13}\}$ triad groups with each triad being composed of three edge-shared $\{MO_6\}$ octahedra, forming a solid metal cluster. The loading number of HIm in every single cell of $HImPMo_{12}$ is 3 (Figures S5 and S6). The powder XRD peaks (Figures 1b and S7) of the as-synthesized compounds before and after proton conductivity measurement are all in good agreement with the corresponding simulated peaks, indicating that the stable POMs keep their structures intact after measurement.

The Fourier transform infrared (FT-IR) spectra of $HImMo_{132}$, $HMeIm_{132}$, $ILMo_{132}$, and $TBAMo_{132}$ are shown in Figure S8. Medium and weak bands in the range of 1650−1100 cm^{-1} as well as strong and medium bands in the range of 1100−400 cm^{-1} are observed. The medium band at 940 cm^{-1} originates from the stretching vibrations of the terminal Mo═O bonds. The strong band at approximately 798 cm^{-1} is associated with the antisymmetric stretching of the Mo−O−Mo bridges, whereas the medium peak at 626 cm^{-1} and the strong peak at 581 cm^{-1} are attributed to the bending vibrations of Mo−O−Mo bridges. Moreover, the peaks in the range of 1550−1400 cm^{-1} correspond to the vibrations of the bridging acetate groups, stabilizing the whole ball structure. Weak to medium bands at approximately 1571 and 1151 cm^{-1} arise from the stretching vibrations of the C═C bonds and bending vibrations of the C−H bond of the imidazole group in $HImMo_{132}$, respectively. The FT-IR spectra (Figures S8 and S9) further prove the fact that the structural integrity of POM is well kept by the compounds before and after the proton conduction measurement. Raman spectra show very characteristic bands for the molybdenum ball species in the region of 150−2000 cm^{-1} (Figure S10).

The proton conductivities were determined via alternating current (AC) impedance spectroscopy. Figure 2a shows the real (Z') and imaginary (Z'') spectra of $HImMo_{132}$ with relative humidity (RH) ranging from 50 to 98% at 25 °C. The Nyquist plots possess a depressed semicircle that could be assigned to bulk and grain boundary resistances and a slanted line related to mobile ions that were hindered by the electrode−electrolyte interfaces.[40] At 50% RH, the conductivity value was measured to be 1.26×10^{-6} S cm^{-1}. With RH increasing, the conductivity gradually increased to 6.19×10^{-3} S cm^{-1} at 98% RH. The σ value increased with the increase of RH as well. We attributed this tendency to the fact that water molecules could supply multiple proton transfer sites, which is beneficial to enhance proton conductivity performance. Upon increasing the temperature from 25 to 60 °C, the conductivity at 98% RH has risen rapidly and reached a value of 4.98×10^{-2} S cm^{-1}, which shows the highest conductivity among the reported POM-based conductors (Figure 2b).[29,36,41−44]

To decipher the number of proton sources in the proton conduction, control experiments on $HMeImMo_{132}$, $ILMo_{132}$, and $TBAMo_{132}$ with the same POM anion and the same crystal water content but with different protonic species have been performed (Figures S12−S20). Incorporation of imidazole molecules as proton-rich N-containing ligands into porous materials was generally considered to be helpful for enhancing their proton conductivity since there are two N atoms on the imidazole molecule: one of the N contains an intrinsic proton H, whereas the other easily accepts H.[20] In comparison, one of the N atoms on the methylimidazole molecule is occupied by a methyl group; yet, only one N can accept protons, so the proton source of methylimidazole is reduced. The two N atoms on the ionic liquid molecule are occupied by a methyl group and a hydroxyethyl group, respectively, wherein the hydroxyethyl group has a proton. However, the bond energy of the O−H bond in the ionic liquid group is greater than that of the N−H bond in the imidazole molecule, resulting in a lower proton concentration of the entire ionic liquid molecule, making it more difficult to form a proton-transport path.[45] There are no protons on the tetrabutylammonium molecule. As the number of protons in compounds $HImMo_{132}$, $HMeImMo_{132}$, $ILMo_{132}$, and $TBAMo_{132}$ decreases, the conductivity of these compounds at 60 °C and 98% RH decreases as well, which are 4.98×10^{-2}, 2.13×10^{-2}, 3.28×10^{-3}, and 1.8×10^{-5} S cm^{-1}, respectively (Figure 2c). $TBAMo_{132}$ shows a remarkably decreased conductivity of 1.8×10^{-5} S cm^{-1}, 3-fold lower than that of $HImMo_{132}$, indicating the scarcity of proton donors. The solid cluster $HImPMo_{12}$ containing the same proton sources shows conductivity (8.35×10^{-3} S cm^{-1}) 1 order of magnitude lower than that of the giant ball $HImMo_{132}$ because the chemically functionalizable pore in $HImMo_{132}$ could be loaded with additional ion carriers and be allowed for the targeted HIm to operate under a wide variety of humidity conditions. To further determine the stability of proton conduction for the as-synthesized compounds, the temperature-dependent conductivity measurements of $HImMo_{132}$ during two heating and cooling cycles with the temperature range of 25−60 °C at 98% RH were carried out (Figures S21 and S22). The conductivity values show good retention during the second cycles, and the cooling−heating conductivity plots were almost linear, showing the stable conductivity performance of $HImMo_{132}$.

To further understand the role of water molecules in creating the proton-conducting pathways in these compounds, water vapor absorption and desorption isotherms for these compounds were measured at 25 °C (Figure S23). As the RH monotonically increased, the σ value increased because H_2O serves as one of the proton-transport vehicle in the form of $H_2O-H_3O^+$. The water absorption−desorption isotherms show that $ILMo_{132}$ (231.10 cm^3 g^{-1}) and $HMeImMo_{132}$ (186.20 cm^3 g^{-1}) exhibit higher water vapor uptake than $HImMo_{132}$ (168.44 cm^3 g^{-1}), resulting from the occupation of free imidazole molecules inside the cavity of $\{Mo_{132}\}$. All hollow ball structures uptake higher water vapor than the solid cluster $HImPMo_{12}$ because the inherent cavities in the hollow structure are favorable for absorbing more water as proton carriers.

DOI: 10.1021/acsami.8b20509
ACS Appl. Mater. Interfaces 2019, 11, 7030−7036

To gain the possible mechanistic insight into proton transfer, temperature-dependent proton conductivity measurements were carried out from 25 to 60 °C under 98% RH. Figure 2d shows the Arrheninus plots of proton conductivities, and E_a of $HImMo_{132}$, $HMeImMo_{132}$, $ILMo_{132}$, $TBAMo_{132}$, and $HImPMo_{12}$ were calculated to be 0.51, 0.44, 0.57, 0.68, and 0.52 eV, respectively. There are two principal mechanisms to explain the proton transportation, the Grotthus mechanism usually with the activation energies lower than 0.4 eV and the vehicle mechanism with the activation energies larger than 0.4 eV.[46] It suggests a vehicular mechanism during the proton transport through these five compounds, where proton transfer is arisen from the diffusion of charged "proton-carrier" molecules (Figure 3). Since the vehicle mechanism no longer requires an infinite hydrogen-bonding network, Im that can behave as a Brønsted base (proton acceptor) is able to bind a proton to form HIm in the amphoteric host lattice. The water molecules are bound to protons to form a complex H_3O^+ inside or outside the channels and act as vehicles. In other words, the vehicles loaded with protons and the "unloaded" vehicles run in the opposite direction, so it requires a higher energy to activate the proton migrating into the compounds.

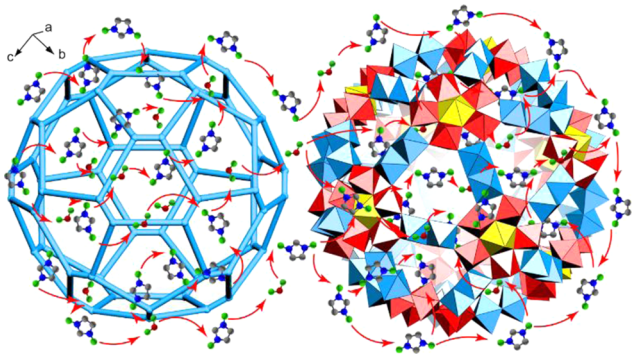

Figure 3. Intramolecular and intermolecular proton-transport mechanisms for $HImMo_{132}$ including proton carriers H_3O^+ and HIm.

$HImMo_{132}$ compounds showing such obvious high proton conductivities are derived from the following factors: (i) polyanion POMs are superacids possessing nucleophilic oxygen-enriched surfaces, which could facilitate proton to change path through migration on the external oxygen atoms of POMs. (ii) The proton conductivity of $HImMo_{132}$ is better than that of $HMeImMo_{132}$, $ILMo_{132}$, and $TBAMo_{132}$ because the N-containing imidazole ligands contain richer proton sources. (iii) When the proton source is the same, the proton conductivity of the hollow ball $HImMo_{132}$ is superior to that to the solid cluster $HImPMo_{12}$. One of the reasons is that the larger pore size and larger surface area of $\{Mo_{132}\}$ can effectively provide channels for proton migration. This is in accord with the fact that the density value calculated from the crystal structure of $HMeImMo_{132}$ (ρ_{calc} = 1.907 g cm^{-3}) is much smaller than the density of $HImPMo_{12}$ (ρ_{calc} = 3.300 g cm^{-3}). In addition, the macroscopic accumulated situation between molecules obtaining from the single-crystal structure is another reason. The nearest distance between neighboring $\{Mo_{132}\}$ molecules is 2.951 Å, which is shorter than that of $\{PMo_{12}\}$ (3.287 Å). It can be concluded that solid proton conductors with a closer packing distance and a shorter diffusion length can provide faster transport pathways for protons. $\{Mo_{132}\}$ possessing such characteristics is favorable for the "vehicle" $-H_3O^+$ and HIm transmission.

4. CONCLUSIONS

In summary, POMs as models simulating the solid-to-hollow structure exhibit excellent proton conductivity and are potential candidates for proton exchange membrane fuel cell (PEMFC) applications. The compounds $HImMo_{132}$, $HMeImMo_{132}$, $ILMo_{132}$, $TBAMo_{132}$, and $HImPMo_{12}$ were synthesized, and their proton conduction mechanisms were studied to explain that the hollow materials can provide more efficient proton transfer paths than solid spheres at the molecular level. Giant POMs as proton conductors were first studied here, displaying advantages over solid spheres due to their strong acidity and the inherent pores and windows within the crystalline structure. The fullerene-type compound $HImMo_{132}$ shows an enhanced proton conductivity of 4.98×10^{-2} S cm^{-1}. It is one of the highest proton conductivities among the reported POM-based conductors. The novel materials we have synthesized here are promising for extending applications in energy conversion and storage. This study not only provides a potential path toward designing and synthesizing new materials in PEMFCs but also offers an ideal crystalline model system toward performance comparison at the molecular level.

■ ASSOCIATED CONTENT

Supporting Information

The Supporting Information is available free of charge on the ACS Publications website at DOI: 10.1021/acsami.8b20509.

Crystallographic datas (CIF) (CIF) (CIF) (CIF)

Experimental methods, related materials' characterization, and proton conductivity; view of structures $HMeImMo_{132}$, $ILMo_{132}$, and $HImPMo_{12}$; view of $HMeImMo_{132}$, $ILMo_{132}$, and $HImPMo_{12}$ packing diagrams; XRD spectra of $HMeImMo_{132}$, $ILMo_{132}$, $TBAMo_{132}$, and $HImPMo_{12}$; FT-IR spectra of $HImMo_{132}$, $HMeImMo_{132}$, $ILMo_{132}$, $TBAMo_{132}$, and PMo_{12}; Raman spectra and TGA profiles of $HImMo_{132}$, $HMeImMo_{132}$, $ILMo_{132}$, $TBAMo_{132}$, and $HImPMo_{12}$; RH dependence of proton conductivity in $HImMo_{132}$, $HMeImMo_{132}$, $HImPMo_{12}$, and $ILMo_{132}$; Nyquist plots of $HMeImMo_{132}$, $HImPMo_{12}$, $ILMo_{132}$, and $TBAMo_{132}$; impedance spectra of $HMeImMo_{132}$, $HImPMo_{12}$, $ILMo_{132}$, and $TBAMo_{132}$; Nyquist plots from AC impedance data; Arrhenius plots of proton conductivity; and H_2O vapor absorption−desorption isotherm (PDF)

■ AUTHOR INFORMATION

Corresponding Author

*E-mail: yqlan@njnu.edu.cn.

ORCID

Long-Zhang Dong: 0000-0002-9276-5101

Ya-Qian Lan: 0000-0002-2140-7980

Author Contributions

†W.-J.L., L.-Z.D., and R.-H.L. contributed equally to this work.

Notes

The authors declare no competing financial interest.

■ ACKNOWLEDGMENTS

This work was financially supported by the National Natural Science Foundation of China (Nos 21701086, 21622104,

21871141, and 21871142), the Postdoctoral Science Foundation of China (No. 2017M621775), and Jiangsu Postdoctoral Research Funds (No. 1701116C). We thank the staff from BL17B beamline of National Facility for Protein Science Shanghai (NFPS) at Shanghai Synchrotron Radiation Facility for assistance during data collection.

■ REFERENCES

(1) Steele, B. C. H.; Heinzel, A. Materials for Fuel-Cell Technologies. *Nature* **2001**, *414*, 345−352.

(2) Jacobson, M. Z.; Colella, W. G.; Golden, D. M. Cleaning the Air and Improving Health with Hydrogen Fuel-Cell Vehicles. *Science* **2005**, *308*, 1901−1905.

(3) Chen, L.; Peng, B.; Wang, J.; Li, D.; Qian, Z.; Xu, G.; Wu, M.; Chen, L.; Shi, G.; Zhang, B.; Wang, Y.; Bian, F.; Li, D.; Zeng, J.; Zhang, L.; Yang, Y.; Li, J.; Fang, H.; Chen, L.; Zhou, G.; Shen, J.; Liu, G.; et al. Ion Sieving in Graphene Oxide Membranes via Cationic Control of Interlayer Spacing. *Nature* **2017**, *550*, 380−383.

(4) Sun, X.-L.; Deng, W.-H.; Chen, H.; Han, H.-L.; Taylor, J. M.; Wan, C.-Q.; Xu, G. A Metal−Organic Framework Impregnated with a Binary Ionic Liquid for Safe Proton Conduction above 100 °C. *Chem. - Eur. J.* **2017**, *23*, 1248−1252.

(5) Yang, F.; Xu, G.; Dou, Y.; Wang, B.; Zhang, H.; Wu, H.; Zhou, W.; Li, J.-R.; Chen, B. A Flexible Metal-Organic Framework with a High Density of Sulfonic Acid Sites for Proton Conduction. *Nat. Energy* **2017**, *2*, 877−883.

(6) Xie, Y.; Shi, N.; Huan, D.; Tan, W.; Zhu, J.; Zheng, X.; Pan, H.; Peng, R.; Xia, C. A Stable and Efficient Cathode for Fluorine-Containing Proton-Conducting Solid Oxide Fuel Cells. *ChemSusChem* **2018**, *11*, 3423−3430.

(7) Cao, L.; Wu, H.; Yang, P.; He, X.; Li, J.; Li, Y.; Xu, M.; Qiu, M.; Jiang, Z. Graphene Oxide-Based Solid Electrolytes with 3D Prepercolating Pathways for Efficient Proton Transport. *Adv. Funct. Mater.* **2018**, *28*, No. 1804944.

(8) Li, F.; Tao, Z.; Dai, H.; Xi, X.; Ding, H. A High-Performing Proton-Conducting Solid Oxide Fuel Cell with Layered Perovskite Cathode in Intermediate Temperatures. *Int. J. Hydrogen Energy* **2018**, *43*, 19757−19762.

(9) Xiang, Y.; Lu, S.; Jiang, S. P. Layer-by-Layer Self-Assembly in the Development of Electrochemical Energy Conversion and Storage Devices from Fuel Cells to Supercapacitors. *Chem. Soc. Rev.* **2012**, *41*, 7291−7321.

(10) Ramaswamy, P.; Wong, N. E.; Shimizu, G. K. H. MOFs as Proton Conductors-Challenges and Opportunities. *Chem. Soc. Rev.* **2014**, *43*, 5913−5932.

(11) Pili, S.; Argent, S. P.; Morris, C. G.; Rought, P.; García-Sakai, V.; Silverwood, I. P.; Easun, T. L.; Li, M.; Warren, M. R.; Murray, C. A.; Tang, C. C.; Yang, S.; Schröder, M. Proton Conduction in a Phosphonate-Based Metal−Organic Framework Mediated by Intrinsic "Free Diffusion inside a Sphere". *J. Am. Chem. Soc.* **2016**, *138*, 6352−6355.

(12) Kim, Y.; Ketpang, K.; Jaritphun, S.; Park, J. S.; Shanmugam, S. A Polyoxometalate Coupled Graphene Oxide-Nafion Composite Membrane for Fuel Cells Operating at Low Relative Humidity. *J. Mater. Chem. A* **2015**, *3*, 8148−8155.

(13) Meng, X.; Wang, H.-N.; Song, S.-Y.; Zhang, H.-J. Proton-conducting Crystalline Porous Materials. *Chem. Soc. Rev.* **2017**, *46*, 464−480.

(14) Miyatake, K.; Chikashige, Y.; Higuchi, E.; Watanabe, M. Tuned Polymer Electrolyte Membranes Based on Aromatic Polyethers for Fuel Cell Applications. *J. Am. Chem. Soc.* **2007**, *129*, 3879−3887.

(15) Bai, H.; Li, Y.; Zhang, H.; Chen, H.; Wu, W.; Wang, J.; Liu, J. Anhydrous Proton Exchange Membranes Comprising of Chitosan and Phosphorylated Graphene Oxide for Elevated Temperature Fuel Cells. *J. Membr. Sci.* **2015**, *495*, 48−60.

(16) Xu, G.; Otsubo, K.; Yamada, T.; Sakaida, S.; Kitagawa, H. Superprotonic Conductivity in a Highly Oriented Crystalline Metal-Organic Framework Nanofilm. *J. Am. Chem. Soc.* **2013**, *135*, 7438−7441.

(17) Zhu, M.; Hao, Z.-M.; Song, X.-Z.; Meng, X.; Zhao, S.-N.; Song, S.-Y.; Zhang, H.-J. A New Type of Double-Chain Based 3D Lanthanide(III) Metal−Organic Framework Demonstrating Proton Conduction and Tunable Emission. *Chem. Commun.* **2014**, *50*, 1912−1914.

(18) Li, X.; Sun, X.; Li, X.; Fu, Z.; Su, Y.; Xu, G. Porous Cadmium(II) Anionic Metal-Organic Frameworks Based on Aromatic Tricarboxylate Ligands: Encapsulation of Protonated Flexible Bis(2-methylimidazolyl) Ligands and Proton Conductivity. *Cryst. Growth Des.* **2015**, *15*, 4543−4548.

(19) Meng, X.; Song, S.-Y.; Song, X.-Z.; Zhu, M.; Zhao, S.-N.; Wu, L.-L.; Zhang, H.-J. A. Tetranuclear Copper Cluster-Based MOF with Sulfonate−Carboxylate Ligands Exhibiting High Proton Conduction Properties. *Chem. Commun.* **2015**, *51*, 8150−8152.

(20) Zhang, F.-M.; Dong, L.-Z.; Qin, J.-S.; Guan, W.; Liu, J.; Li, S.-L.; Lu, M.; Lan, Y.-Q.; Su, Z.-M.; Zhou, H.-C. The Effect of Imidazole Arrangements on Proton-Conductivity in Metal-Organic Frameworks. *J. Am. Chem. Soc.* **2017**, *139*, 6183−6189.

(21) Bae, J.; Choi, J. S.; Hwang, S.; Yun, W. S.; Song, D.; Lee, J.; Jeong, N. C. Multiple Coordination Exchanges for Room-Temperature Activation of Open-Metal Sites in Metal−Organic Frameworks. *ACS Appl. Mater. Interfaces* **2017**, *9*, 24743−24752.

(22) Kim, S. B.; Kim, J. Y.; Jeong, N. C.; Ok, K. M. Anisotropic Li^+ Ion Conductivity in a Large Single Crystal of a Co(III) Coordination Complex. *Inorg. Chem. Front.* **2017**, *4*, 79−83.

(23) Hwang, S.; Lee, E. J.; Song, D.; Jeong, N. C. High Proton Mobility with High Directionality in Isolated Channels of MOF-74. *ACS Appl. Mater. Interfaces* **2018**, *10*, 35354−35360.

(24) Yuan, Y.-Y.; Yang, S.-L.; Zhang, C.; Wang, Q.-L. A New Europium Metal-Organic Framework with both High Proton Conductivity and Highly Sensitivity Detection of Ascorbic Acid. *CrystEngComm* **2018**, *20*, 6989−6994.

(25) Bae, J.; Lee, E. J.; Jeong, N. C. Metal Coordination and Metal Activation Abilities of Commonly Unreactive Chloromethanes toward Metal−Organic Frameworks. *Chem. Commun.* **2018**, *54*, 6458−6471.

(26) Zang, H.-Y.; Chen, J.-J.; Long, D.-L.; Cronin, L.; Miras, H. N. Assembly of Thiometalate-Based $\{Mo_{16}\}$ and $\{Mo_{36}\}$ Composite Clusters Combining $[Mo_2O_2S_2]^{2+}$ Cations and Selenite Anions. *Adv. Mater.* **2013**, *25*, 6245−6249.

(27) Liu, Y.; Liu, S.; Lai, X.; Miao, J.; He, D.; Li, N.; Luo, F.; Shi, Z.; Liu, S. Polyoxometalate-Modified Sponge-Like Graphene Oxide Monolith with High Proton-Conducting Performance. *Adv. Funct. Mater.* **2015**, *25*, 4480−4485.

(28) Zang, H.-Y.; Chen, J.-J.; Long, D.-L.; Cronin, L.; Miras, H. N. Assembly of Inorganic $[Mo_2S_2O_2]^{2+}$ Panels Connected by Selenite Anions to Nanoscale Chalcogenide-Polyoxometalate Clusters. *Chem. Sci.* **2016**, *7*, 3798−3804.

(29) Liu, J.-C.; Han, Q.; Chen, L.-J.; Zhao, J.-W.; Streb, C.; Song, Y.-F. Aggregation of Giant Cerium−Bismuth Tungstate Clusters into a 3D Porous Framework with High Proton Conductivity. *Angew. Chem., Int. Ed.* **2018**, *57*, 8416−8420.

(30) Wang, J.-X.; Wang, Y.-D.; Wei, M.-J.; Tan, H.-Q.; Wang, Y.-H.; Zang, H.-Y.; Li, Y.-G. Inorganic Open Framework based on Lanthanide Ions and Polyoxometalates with High Proton Conductivity. *Inorg. Chem. Front.* **2018**, *5*, 1213−1217.

(31) Wang, Y.-D.; Wang, J.-X.; Wei, M.-J.; Liu, B.-L.; Zang, H.-Y.; Tan, H.-Q.; Wang, Y.-H.; Li, Y.-G. Niobium Oxyhydroxide-Polyoxometalate Composite as an Efficient Proton-Conducting Solid Electrolyte. *ChemElectroChem* **2018**, *5*, 1125−1129.

(32) Motz, A. R.; Kuo, M.-C.; Horan, J. L.; Yadav, R.; Seifert, S.; Pandey, T. P.; Galioto, S.; Yang, Y.; Dale, N. V.; Hamrock, S. J.; Herring, A. M. Heteropoly Acid Functionalized Fluoroelastomer with Outstanding Chemical Durability and Performance for Vehicular Fuel Cells. *Energy Environ. Sci.* **2018**, *11*, 1499−1509.

(33) Nakamura, O.; Kodama, T.; Ogino, I.; Miyake, Y. High-Conductivity Solid Proton Conductors: Dodecamolybdophosphoric

DOI: 10.1021/acsami.8b20509
ACS Appl. Mater. Interfaces 2019, 11, 7030−7036

Acid and Dodecatungstophosphoric Acid Crystals. *Chem. Lett.* **1979**, *8*, 17−18.
(34) Gumerova, N. I.; Rompel, A. Synthesis, Structures and Applications of Electron-Rich Polyoxometalates. *Nat. Rev. Chem.* **2018**, *2*, 0112.
(35) Liu, W.-J.; Yu, G.; Zhang, M.; Li, R.-H.; Dong, L.-Z.; Zhao, H.-S.; Chen, Y.-J.; Xin, Z.-F.; Li, S.-L.; Lan, Y.-Q. Investigation of the Enhanced Lithium Battery Storage in a Polyoxometalate Model: From Solid Spheres to Hollow Balls. *Small Methods* **2018**, *2*, No. 1800154.
(36) Cao, X.-L.; Xie, S.-L.; Li, S.-L.; Dong, L.-Z.; Liu, J.; Liu, X.-X.; Wang, W.-B.; Su, Z.-M.; Guan, W.; Lan, Y.-Q. A Well-Established POM-based Single-Crystal Proton-Conducting Model Incorporating Multiple Weak Interactions. *Chem. - Eur. J.* **2018**, *24*, 2365−2369.
(37) Liu, Y.; Yang, X.; Miao, J.; Tang, Q.; Liu, S.; Shi, Z.; Liu, S. Polyoxometalate-Functionalized Metal-Organic Frameworks with Improved Water Retention and Uniform Proton-Conducting Pathways in Three Orthogonal Directions. *Chem. Commun.* **2014**, *50*, 10023−10026.
(38) Zeng, J.; Jiang, S. P. Characterization of High-Temperature Proton-Exchange Membranes Based on Phosphotungstic Acid Functionalized Mesoporous Silica Nanocomposites for Fuel Cells. *J. Phys. Chem. C* **2011**, *115*, 11854−11863.
(39) Müller, A.; Krickemeyer, E.; Bögge, H.; Schmidtmann, M.; Peters, F. Organizational Forms of Matter: An Inorganic Super Fullerene and Keplerate Based on Molybdenum Oxide. *Angew. Chem., Int. Ed.* **1998**, *37*, 3359−3363.
(40) Nagarkar, S. S.; Unni, S. M.; Sharma, A.; Kurungot, S.; Ghosh, S. K. Two-in-One: Inherent Anhydrous and Water-Assisted High Proton Conduction in a 3D Metal−Organic Framework. *Angew. Chem., Int. Ed.* **2014**, *53*, 2638−2642.
(41) Li, J.; Cao, X.-L.; Wang, Y.-Y.; Zhang, S.-R.; Du, D.-Y.; Qin, J.-S.; Li, S.-L.; Su, Z.-M.; Lan, Y.-Q. The Enhancement on Proton Conductivity of Stable Polyoxometalate-Based Coordination Polymers by the Synergistic Effect of MultiProton Units. *Chem. - Eur. J.* **2016**, *22*, 9299−9304.
(42) Ma, P.; Wan, R.; Wang, Y.; Hu, F.; Zhang, D.; Niu, J.; Wang, J. Coordination-Driven Self-Assembly of a 2D Graphite-Like Framework Constructed from High-Nuclear Ce_{10} Cluster Encapsulated Polyoxotungstates. *Inorg. Chem.* **2016**, *55*, 918−924.
(43) Gao, Q.; Wang, X.-L.; Xu, J.; Bu, X.-H. The First Demonstration of the Gyroid in a Polyoxometalate-Based Open Framework with High Proton Conductivity. *Chem. - Eur. J.* **2016**, *22*, 9082−9086.
(44) Li, Z.; Li, X.-X.; Yang, T.; Cai, Z.-W.; Zheng, S.-T. Four-Shell Polyoxometalates Featuring High-Nuclearity Ln_{26} Clusters: Structural Transformations of Nanoclusters into Frameworks Triggered by Transition-Metal Ions. *Angew. Chem., Int. Ed.* **2017**, *56*, 2664−2669.
(45) Cotton, F. A.; Wilkinson, G.; Murillo, C. A.; Bochmann, M. *Advanced Inorganic Chemistry*, 3rd ed.; John Wiley & Sons, Inc.: New York, 1999.
(46) Kreuer, K.-D.; Rabenau, A.; Weppner, W. Vehikel-Mechanismus, ein neues Modell zur Deutung der Leitfähigkeit schneller Protonenleiter. *Angew. Chem.* **1982**, *94*, 224−225.

DOI: 10.1021/acsami.8b20509
ACS Appl. Mater. Interfaces 2019, 11, 7030−7036